PHYSICAL REVIEW B VOLUME 25, NUMBER 6 15 MARCH 1982

Complex band structures of crystalline solids: An eigenvalue method

Yia-Chung Chang and J. N. Schulman*
Department of Physics and Materials Research Laboratory, University of Illinois at Urbana-Champaign, Urbana, Illinois 61801
(Received 13 October 1981)

A general method for calculating the complex band structures of solids is presented. This method is adaptable to the pseudopotential, full-zone $\vec{k}\cdot\vec{p}$, and tight-binding formalisms. The basic idea is to express the total Hamiltonian of the bulk material as a polynomial in a simple analytic function of the wave vector perpendicular to a given plane. A companion matrix associated with this polynomial is constructed, and then diagonalized. The resulting eigenvalues and eigenvectors give rise to the complex band structure and the evanescent Bloch states. Using these evanescent states, the bulk Green's function for fixed $\bar{k}$ (wave vector parallel to the given plane) can be obtained from a simple analytic expression; thus the study of electronic properties associated with a planar defect in the solid is facilitated. For illustrative purposes, we present the complex band structure of Si calculated within the three different schemes and compare them. We also compute the bulk Green's function (with fixed $\bar{k}$) and find the surface states for the ideal Si (100), (111), and (110) faces within the tight-binding formalism.

I. INTRODUCTION

Bulk evanescent states (Bloch states associated with complex values of the wave vector, $\vec{k}$) play a significant role in determining the electronic properties of solids with planar defects (e.g., surfaces, interfaces, stacking faults, and superlattices). There have been several theoretical studies on solid surfaces,[1-3] interfaces,[4] and superlattices[5] using the matching method in which the total wave function is expanded in terms of bulk propagating and evanescent states on both sides of a matching plane. The coefficients of expansion are determined by solving the Schrödinger equation with appropriate boundary conditions. This method has considerable advantage over the other theoretical techniques, including the slab method[6] and Koster-Slater method,[7,8] in its simplicity and numerical efficiency. In fact, knowing the evanescent states for each fixed energy E and wave vector parallel to the matching plane $\bar{k}$ is equivalent to knowing the Green's function for the bulk materials. Using the evanescent states, the bulk Green's function with fixed $\bar{k}$ can be evaluated more precisely and efficiently.[9]

In a previous paper, one of us (Y.C.C.) reported on calculations of the complex band structures of 14 zinc-blende materials.[10] In Ref. 10, the complex k_z values for each fixed E and $\bar{k}$ are obtained by finding the zeros of the polynomial obtained from the determinant of $(H-E)$ (H is the Hamiltonian of the solid). Although this method is quite simple and efficient, it has numerical difficulties when the order of the polynomial becomes large. In the present paper, we introduce a more general method for obtaining the evanescent states. In this method the complex wave vectors for fixed E and $\bar{k}$ are obtained by diagonalizing a "companion matrix" constructed from the Hamiltonian, H. This method is applicable for the pseudopotential and full zone $\vec{k}\cdot\vec{p}$ schemes as well as the tight-binding scheme. The tight-binding version of this method was used in Ref. 5.

The basic idea of our method is simple. In all three schemes the Schrödinger equation for the solid can be converted into a polynomial equation in a variable which is some simple analytic function of k_z. The coefficients of this polynomial are finite-dimensional matrices for a Bloch function expanded in a finite basis set. The roots of the polynomial, which contain the information about the evanescent states, can be obtained by diagonalizing an associated "companion matrix."

This paper is organized as follows: In Sec. II, we present the general method for obtaining the complex band structures of solids. All three commonly used schemes, including tight-binding, $\vec{k}\cdot\vec{p}$, and pseudopotential, are discussed. In Sec. III, we illustrate the use of the present method by calculating the complex band structure of Si in the three

different schemes and comparing them. In Sec. IV, we discuss one application of the complex band structures to solid surfaces. We use the evanescent states to calculate the bulk Green's function with fixed $\bar{k}$ and then calculate the surface states of the ideal Si (100), (111) and (110) surfaces according to the expression given by Allen,[9] within the tight-binding formalism. In Sec. V a summary is presented.

II. GENERAL THEORY

To find the evanescent states associated with a given planar defect (surface or interface) in a solid, we seek the complex wave vectors, $\vec{k}$, which satisfy the Schrödinger equation with energy E,

$$H\psi(\vec{k},\vec{r})=E\psi(\vec{k},\vec{r}) , \tag{1}$$

where H is the total Hamiltonian and $\psi(\vec{k},\vec{r})$ is the Bloch function for the perfect solid. The method for finding the evanescent states can be described in tight-binding, pseudopotential, and $\vec{k}\cdot\vec{p}$ schemes, which we shall discuss separately in the following sections.

A. Tight-binding scheme

To study the problem associated with a planar defect in a tight-binding scheme, we first introduce the basic terminology to be used in this section: A layer is defined to be a collection of atomic planes parallel to the defect plane (DP) which form a unit cell when the solid is viewed as a linear chain perpendicular to the DP. A planar orbital is defined as the sum of atomic orbitals (labeled α) in the i^{th} atomic plane of a given layer, weighted by the phase factor $e^{i\bar{k}\cdot\bar{R}}$, i.e.,

$$|\alpha i;\bar{k}l_z\rangle=\sum_{\bar{R}} e^{i\bar{k}\cdot\bar{R}}|\alpha i;\vec{R}\rangle , \tag{2}$$

where $\bar{k}$ and $\bar{R}$ are the wave vector and lattice positions ($\vec{R}$) projected on the DP, l_z denotes the layer position, and $|\alpha i;\vec{R}\rangle$ is the atomic orbital centered at $\vec{R}$.

In the present scheme, the Bloch state $|\psi(\bar{k},k_z)\rangle$ is expanded in terms of a linear combination of the planar orbitals,

$$|\psi(\bar{k}k_z)\rangle=\sum_{\alpha i} C_{\alpha i}(\bar{k}k_z) \times\left[\frac{1}{\sqrt{N}}\sum_{l_z} e^{ik_z l_z}|\alpha i;\bar{k}l_z\rangle\right] , \tag{3}$$

where the $C_{\alpha i}$ are the expansion coefficients and N is a normalization constant. In the planar orbital basis, the Schrödinger equation [Eq. (1)] is written as

$$\sum_{\alpha i}\langle\alpha' i';\bar{k}l_z|\bar{H}|\alpha i;k_z\rangle C_{\alpha i}=0 , \tag{4}$$

where $|\alpha i;k_z\rangle$ denotes the states in the large parentheses of Eq. (3) including the summation over l_z, and

$$\langle\alpha' i';\bar{k}l_z|\bar{H}|\alpha i;k_z\rangle\equiv\langle\alpha' i';\bar{k}l_z|H|\alpha i;k_z\rangle -E\langle\alpha i;\bar{k}l_z|\alpha i;k_z\rangle .$$

To keep the theory general, we do not restrict the tight-binding basis states to form an orthonormal set. It should be noted that Eq. (4) is independent of l_z, because of the translational invariance of $\bar{H}$.

If we truncate the matrix elements of $\bar{H}$ in Eq. (4) at some finite number of neighbors, we find that each of them can be written as a polynomial in $e^{ik_z a'}$ with a' being the distance between two adjacent layers, viz.,

$$\bar{H}(\vec{k})=\sum_{\sigma=-m}^{m}\bar{H}^{(\sigma)}(\bar{k})e^{i\sigma k_z a'} , \tag{5}$$

where m is the number of neighboring layers included. In Eq. (5), we have omitted the indices (αi) and expressed the k_z dependence explicitly. $\bar{H}^{(\sigma)}(\bar{k})$, represents a matrix which couples a given layer to the σth neighboring layer. We define

$$C_{\alpha i}^{(\sigma)}\equiv e^{i\sigma k_z a'}C_{\alpha i} , \quad \sigma=-m,\ldots,m . \tag{6}$$

Substituting Eqs. (5) and (6) into Eq. (4) yields

$$\sum_{\sigma=-m}^{m-1}\bar{H}^{(\sigma)}C^{(\sigma)}+\bar{H}^{(m)}e^{ik_z a'}C^{(m-1)}=0 , \tag{7}$$

where $C^{(m)}$ has been expressed as $e^{ik_z a'}C^{(m-1)}$.

Also note that

$$C^{(\sigma)}=e^{ik_z a'}C^{(\sigma-1)} , \quad \sigma=-m+1,\ldots,m-1 . \tag{8}$$

In Eqs. (7) and (8), we have also omitted the subscripts αi. Equation (7) multiplied by $\bar{H}^{(m)-1}$ and Eq. (8) lead to an eigenvalue equation for $e^{ik_z a'}$,[11]

$$\begin{bmatrix} -\bar{H}^{(m)-1}\bar{H}^{(m-1)} & \cdots & -\bar{H}^{(m)-1}\bar{H}^{(0)} & \cdots & -\bar{H}^{(m)-1}\bar{H}^{(-m)} \\ 1_0 & \cdots & 0 & \cdots & 0 \\ 0 & 1_0 \cdots & 0 & \cdots & 0 \\ \cdot & \cdots & \cdot & \cdots & \cdot \\ \cdot & \cdots & \cdot & \cdots & \cdot \\ \cdot & \cdots & 1_0 & \cdots & \cdot \\ \cdot & \cdots & \cdot & \cdots & \cdot \\ \cdot & \cdots & \cdot & \cdots & \cdot \\ 0 & \cdots & 0 & \cdots 1_0 & 0 \end{bmatrix} \begin{bmatrix} C^{(m-1)} \\ C_{(m-2)} \\ \cdot \\ \cdot \\ C^{(0)} \\ \cdot \\ \cdot \\ \cdot \\ C^{(-m)} \end{bmatrix} = e^{ik_z a'} \begin{bmatrix} \bar{C}^{(m-1)} \\ \bar{C}^{(m-2)} \\ \cdot \\ \cdot \\ C^{(0)} \\ \cdot \\ \cdot \\ \cdot \\ C^{(-m)} \end{bmatrix} . \tag{9}$$

We shall refer to the matrix on the left side of Eq. (9) as the companion matrix (denoted T) of the polynomial $\bar{H}(\vec{k})$. The elements in the second diagonal of T (designated 1_0) represent identity matrices of the same dimension as $\bar{H}$.

Equation (9) is valid whenever the inverse of the matrix $\bar{H}^{(m)}$ exists. In some cases this does not occur and Eq. (9) must be modified. For example, if each layer contains several (say s) atomic planes and the number of neighboring atomic planes coupled by the Hamiltonian to a given plane is less than sm, the $\bar{H}^{(m)}$ will be singular.

Consider the general case in which s' ($s'<s$) atomic planes in the mth layer are not coupled to any atomic planes in the zeroth layer (see Fig. 1). We can write the matrices $\bar{H}^{(\sigma)}$ and column vectors $C^{(\sigma)}$ of Eq. (7) in the following decomposed form,

$$\bar{H}^{(\sigma)} = \begin{bmatrix} \bar{H}_{11}^{(\sigma)} & \cdots & \bar{H}_{1s}^{(\sigma)} \\ \vdots & & \vdots \\ \bar{H}_{s1}^{(\sigma)} & \cdots & \bar{H}_{ss}^{(\sigma)} \end{bmatrix} \tag{10}$$

and

$$C^{(\sigma)} = \begin{bmatrix} C_1^{(\sigma)} \\ \vdots \\ C_s^{(\sigma)} \end{bmatrix} ,$$

where the submatrix $\bar{H}_{ij}^{(\sigma)}$ denotes the coupling between the ith and jth atomic planes in the zeroth and σth layer, respectively. The subcolumn vector $C_i^{(\sigma)}$ contains the expansion coefficients $C_{\alpha i}^{(\sigma)}$ as its components. For the mth layer, the matrix $\bar{H}^{(m)}$ takes the special form

$$\bar{H}^{(m)} = \begin{bmatrix} 0 & 0 \\ h^{(m)} & 0 \end{bmatrix} ,$$

where $h^{(m)}$ is a nonsingular $(s-s')\times(s-s')$ block matrix defined by

$$\begin{bmatrix} \bar{H}_{s'+1,1}^{(m)} & 0 & \cdot & \cdot & 0 \\ \bar{H}_{s'+2,1}^{(m)} & \bar{H}_{s'+2,1}^{(m)} & 0 & \cdot & \cdot \\ \cdot & \cdot & \cdot & 0 & \cdot \\ \cdot & \cdot & \cdot & \cdot & 0 \\ \bar{H}_{s,1}^{(m)} & \cdot & \cdot & \cdot & \bar{H}_{s,s-s'}^{(m)} \end{bmatrix} \tag{11}$$

After the decomposition, Eq. (7) can be written as

$$\sum_{\sigma=-m}^{m-1} \left[\sum_{j=1}^{s} \bar{H}_{ij}^{(\sigma)} C_j^{(\sigma)} \right] = 0 , \quad i = 1,..,s' \tag{12}$$

and

$$\sum_{\sigma=-m}^{m-1} \left[\sum_{j=1}^{s} \bar{H}_{ij}^{(\sigma)} C_j^{(\sigma)} \right] + \sum_{j=1}^{s-s'} h_{ij}^{(m)} \left[e^{ik_z a'} C_j^{(m-1)} \right] = 0 ,$$

$$i = s'+1, \ldots, s . \tag{13}$$

Multiplying Eq. (12) by $e^{ik_z a'}$ and using the relation (8), we obtain

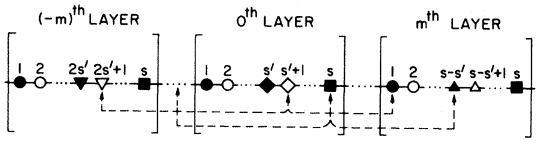

FIG. 1. Coupling between atomic planes in various layers. The coupling is truncated at the $(sm-s')$th neighbor. The arrows indicate the furthermost couplings from various atomic planes in the zeroth layer.

$$\sum_{\sigma=-m+1}^{m-1}\left[\sum_{j=1}^{s}\bar{H}_{ij}^{(\sigma-1)}C_j^{(\sigma)}\right]+\sum_{j=1}^{s}\bar{H}_{ij}^{(m-1)}\left[e^{ik_z a'}C_j^{(m-1)}\right]=0\,,\quad i=1,..,s'\,. \tag{14}$$

Equations (13) and (14) represent s coupled linear equations for the s unknowns $e^{ik_z a'}C_j^{(m-1)}$, $j=1,..,s$. To solve this set of coupled equations for the first $(s-s')$ unknowns we multiply Eq. (13) by $h^{(m)-1}$ and obtain

$$e^{ik_z a'}C_i^{(m-1)}=-\sum_{\sigma=-m}^{m-1}\sum_{i'=s'+1}^{s}\sum_{j=1}^{s}(h^{(m)-1})_{ii'}\bar{H}_{i'j}^{(\sigma)}C_j^{(\sigma)}\,,\quad i=1,\ldots,s-s'\,. \tag{15}$$

To solve for the remaining unknowns, we substitue Eq. (15) into Eq. (14) and obtain

$$e^{ik_z\sigma'}C_i^{(m-1)}=-\sum_{i''=1}^{s'}(h^{(m-1)-1})_{ii''}\sum_{\sigma=-m}^{m-1}\sum_{j=1}^{s}\left[\bar{H}_{i''j}^{(\sigma-1)}-\sum_{j'=1}^{s-s'}\bar{H}_{i''j'}^{(m-1)}\sum_{i'=s'+1}^{s}(h^{(m)-1})_{j'i'}\bar{H}_{i'j}^{(\sigma)}\right]C_j^{(\sigma)}$$

$$i=s-s'+1,\ldots,s\,, \tag{16}$$

where $h^{(m-1)}$ is a nonsingular $s'\times s'$ block matrix with components given by $h_{ij}^{(m-1)}=\bar{H}_{ij}^{(m-1)}$; $i=s-s'+1,\ldots,s$ and $j=1,\ldots,s'$. In Eq. (16) we have defined $\bar{H}^{(-m-1)}\equiv 0$ in order to simplify the expression. Equations (15), (16), and (8) lead to a new eigenvalue equation, which is similar in form to Eq. (9). The resulting companion matrix associated with this eigenvalue equation can be truncated by eliminating the last $2s'M$ rows and columns, where M is the number of independent atomic orbitals in each atomic plane. The last $2s'M$ columns all contain zeros, because Eqs. (15) and (16) relate at most $2(sm-s')+1$ atomic planes (see Fig. 1).

Recently, Lee and Joannopoulos[12] have developed a simple scheme for calculating surface states and surface Green's functions. In their method the surface Green's function is related to a transfer matrix which can also be written directly in terms of tight-binding coupling matrices. The eigenvalues of their transfer matrix also give rise to the complex solutions to the bulk Schrödinger equation. The companion matrix derived in the present paper is closely related to their transfer matrix. Both the companion matrix and the transfer matrix have the same dimension, $2(sm-s')M$. Our companion matrix links each layer (containing s atomic planes) to its adjacent layer, whereas the transfer matrix links two neighboring principal layers [each containing $n=(sm-s')$ atomic planes] in one superlayer to the corresponding principal layers in the adjacent superlayer. Here, a principal layer is defined as the smallest group of atomic planes such that only nearest-neighbor interactions between principal layers exist, and a superlayer is the smallest collection of principal layers, which form a unit cell of a periodic array.[12] For the simplest case ($m=1$), the two matrices are equivalent and both have eigenvalues $e^{ik_z a'}$. For more complicated cases ($m>1$) the companion matrix is computationally simpler in that it contains the inverse of a smaller $((s-s')M\times(s-s')M)$ matrix, while the transfer matrix contains the inverse of a $nM\times nM$ matrix. In these cases, the eigenvalues of the transfer matrix will be powers of $e^{ik_z a'}$.

B. Pseudopotential and $\vec{k}\cdot\vec{p}$ schemes

In the pseudopotential scheme, the Bloch function $\psi(\vec{k},\vec{r})$ is expanded in terms of plane waves, i.e.,

$$\psi(\vec{k},\vec{r})=e^{i\vec{k}\cdot\vec{r}}\sum_{\vec{G}}C(\vec{k},\vec{G})e^{i\vec{G}\cdot\vec{r}}$$

where the $\vec{G}$ are reciprocal-lattice vectors. The Schrödinger equation written in the plane-wave basis is[13]

$$\sum_{\vec{G}'}\bar{H}_{\vec{G},\vec{G}'}(\vec{k})C(\vec{k},\vec{G}')=0\,, \tag{17}$$

where

$$\bar{H}_{\vec{G},\vec{G}'}(\vec{k})\equiv[(\vec{k}+\vec{G})^2-E]\delta_{\vec{G},\vec{G}'} + V(|\vec{G}-\vec{G}'|), \quad (18)$$

with $V(|\vec{G}|)$ being the pseudopotential form factors. In Eq. (13) we have introduced the atomic units in which energy and distance are measured in rydbergs and bohrs, respectively.

In the full-zone $\vec{k}\cdot\vec{p}$ perturbation scheme,[14] the Bloch function $\psi(\vec{k},\vec{r})$ is expanded in terms of Bloch functions with associated $\vec{k}=0$ [denoted $u_\nu(\vec{r})$]; i.e.,

$$\psi(\vec{k},\vec{r})=e^{i\vec{k}\cdot\vec{r}}\sum_\nu C_\nu(\vec{k})u_\nu(\vec{r}) . \quad (19)$$

In the $\{u_\nu(\vec{r})\}$ basic, the Schrödinger equation takes the form

$$\bar{H}_{\nu\nu'}(\vec{k})C_{\nu'}(\vec{k})=0 , \quad (20)$$

where

$$\bar{H}_{\nu\nu'}(\vec{k})\equiv(k^2+E_\nu-E)\delta_{\nu\nu'} + 2\langle u_\nu|\vec{k}\cdot\vec{p}|u_{\nu'}\rangle \quad (21)$$

and the E_ν's are energies associated with the $\vec{k}=0$ Bloch states, u_ν.

It is noted that both the $\bar{H}$ matrices in Eqs. (18) and (21) are a quadratic polynomial in k_z for fixed $\bar{k}$ and E. We can simply write

$$\bar{H}(\vec{k})=\bar{H}^{(0)}(\bar{k})+H^{(1)}(\bar{k})k_z+k_z^2 . \quad (22)$$

Equations (17) and (20) can be immediately transformed into an eigenvalue equation for k_z,[15] viz.,

$$\begin{bmatrix} 0 & 1 \\ -\bar{H}^{(0)}(\bar{k}) & -\bar{H}^{(1)}(\bar{k}) \end{bmatrix}\begin{bmatrix} C \\ C^{(1)} \end{bmatrix}=k_z\begin{bmatrix} C \\ C^{(1)} \end{bmatrix}, \quad (23)$$

where $C^{(1)}\equiv k_z C$, and C represents a column vector consisting of the C_ν's.

Previous calculations of the complex band structures of solids within the pseudopotential scheme[2,3] involve finding the zeros of the secular determinant, $\det[\bar{H}(\vec{k})]$ by iterative procedures. This is much more time consuming and less convenient than the present eigenvalue method. Furthermore, it is quite difficult to find all of the correct k_z solutions in the complex k_z plane, unless their values are already approximately known. The present method allows one to obtain all of the complex k_z solutions for fixed E and $\bar{k}$ from diagonalizing a single matrix.

III. COMPLEX BAND STRUCTURES OF Si IN VARIOUS SCHEMES

We have studied the complex band structures of Si within the nearest-neighbor tight-binding, the full zone $\vec{k}\cdot\vec{p}$, and the pseudopotential schemes. In the tight-binding scheme, we have used five atomic orbitals for each atom, including sp^3 plus an excited s-like state. The parameters for this model are given in Ref. 16. The Hamiltonian matrix (in the planar orbital basis) subtracting the energy E can be written as

$$\bar{H}=\begin{bmatrix} \bar{A} & V(\vec{k}) \\ V'(\vec{k}) & \bar{C} \end{bmatrix}, \quad (24)$$

where $\bar{A}$ and $\bar{C}$ are 5×5 diagonal matrices containing the differences between the on-site energy parameters and the energy E. $V(\vec{k})$ and $V'(\vec{k})$ are 5×5 nearest-neighbor coupling matrices, which can be written as polynomials in $e^{ik_z a'}$, viz.,

$$V(\vec{k})=V_-(\bar{k})e^{-ik_z a'}+V_0(\bar{k})+V_+(\bar{k})e^{ik_z a'} \quad (25a)$$

and

$$V'(\vec{k})=V_+^\dagger(\bar{k})e^{-ik_z a'}+V_0^\dagger(\bar{k})+V_-^\dagger(\bar{k})e^{ik_z a'} , \quad (25b)$$

where $V_i^\dagger$ is the Hermitian conjugate of V_i for $i=0$, $+$, and $-$.

For the (110) face, the present example has $m=1$, $s=1$, $s'=0$, and $M=10$. Substituting Eqs. (24) and (25) into Eq. (9), we obtain an eigenvalue equation

$$\begin{bmatrix} -\bar{H}^{(+)-1}\bar{H}^{(0)} & -H^{(+)-1}H^{(-)} \\ 1_0 & 0 \end{bmatrix}\begin{bmatrix} C^{(1)} \\ C^{(0)} \end{bmatrix} = e^{ik_z a'}\begin{bmatrix} C^{(1)} \\ C^{(0)} \end{bmatrix}, \quad (26a)$$

with

$$\bar{H}^{(\pm)}\equiv\begin{bmatrix} 0 & V_\pm(\bar{k}) \\ V_\pm^\dagger(\bar{k}) & 0 \end{bmatrix} \quad (26b)$$

and

$$\bar{H}^{(0)}\equiv\begin{bmatrix} \bar{A} & V_0(\bar{k}) \\ V_0^\dagger(\bar{k}) & \bar{C} \end{bmatrix} . \quad (26c)$$

For the (100) and (111) faces, we have $m=1$, $s=2$, $s'=1$, and $M=5$. In this case, $V_+(\bar{k})=0$ and the inverse of $\bar{H}^{(+)}$ does not exist. Following the procedures discussed in the preceding section [Eqs. (10)–(16)], we obtain another eigenvalue equation

$$\begin{bmatrix} -(V_-^\dagger)^{-1}V_0^\dagger & -(V_-^\dagger)^{-1}\bar{C} \\ V_0^{-1}\bar{A}(V_-^\dagger)^{-1}V_0^+ & V_0^{-1}[\bar{A}(V_-^\dagger)^{-1}\bar{C}-V_-] \end{bmatrix}\begin{bmatrix} C_1 \\ C_2 \end{bmatrix} = e^{ik_z a'}\begin{bmatrix} C_1 \\ C_2 \end{bmatrix} . \quad (27)$$

The complex band structures obtained by diagonalizing the companion matrices given in Eqs. (26) and (27) are shown in Figs. 2–4 for the Si [100], [111], and [110] directions, respectively. In these figures, the purely imaginary ($\mathrm{Re}k_z=0$) and real ($\mathrm{Im}k_z=0$) bands are denoted by solid curves and are plotted in the left and right panels, respectively. The complex bands ($\mathrm{Re}k_z\neq 0$ and $\mathrm{Im}k_z\neq 0$) are denoted by pairs of dashed curves, with their real and imaginary portions plotted in the right and left panels, respectively. We distinguish the bands with $\mathrm{Re}k_z$ located at the zone edge (i.e., $\mathrm{Re}k_z a'=\pi$) from those with general values of $\mathrm{Re}k_z$ by denoting the former and the latter by short and long dashed lines, respectively. Here and after, we refer to them as the "imaginary bands of the second kind" and the "complex bands," respectively.

In the $\vec{k}\cdot\vec{p}$ and pseudopotential schemes, we use the parameters given by Refs. 14 and 13, respectively. The present pseudopotential model includes 89 plane waves (truncated at the seventh shell). The complex band structures for the Si [100], [111], and [110] cases obtained in these two schemes are plotted in Figs. 5–10. The notations used to denote the real, imaginary and complex bands are the same as in Figs. 2–4. In Figs. 5–10, there are many complex k_z solutions whose real parts are found to lie outside the first Brillouin zone. These solutions should be equal to the solutions obtained inside the first Brillouin zone plus a reciprocal-lattice vector. However, since a complete set of basis functions is not used, they are only approximate, repeated-zone scheme solutions. Farther away from the first Brillouin zone, the approximation to the correct solutions becomes worse. Therefore, many complex bands whose real part is outside of the first Brillouin zone have to be discarded. In Figs. 5–7, the bands to be discarded are denoted by dotted lines. In Figs. 8–10, these bands are simply excluded.

Comparing the complex band structures obtained within the three different schemes, we first note that in the pseudopotential scheme there are many complex bands associated with large imaginary k_z

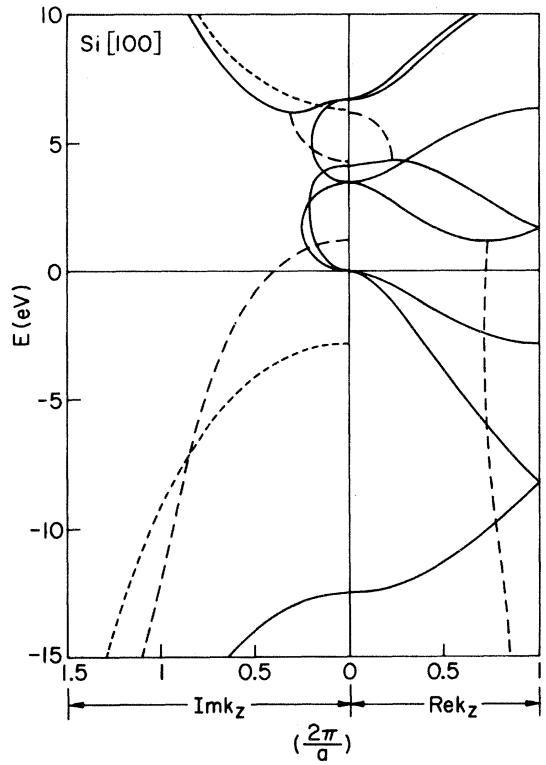

FIG. 2. Complex band structure of Si along [100] direction obtained in the tight-binding scheme. Solid curves denote real bands (right) and imaginary bands (left), short-dashed curves denote complex bands with $\mathrm{Re}k_z$ located at the zone boundary, and long-dashed curves denote complex bands with general values of $\mathrm{Re}k_z$.

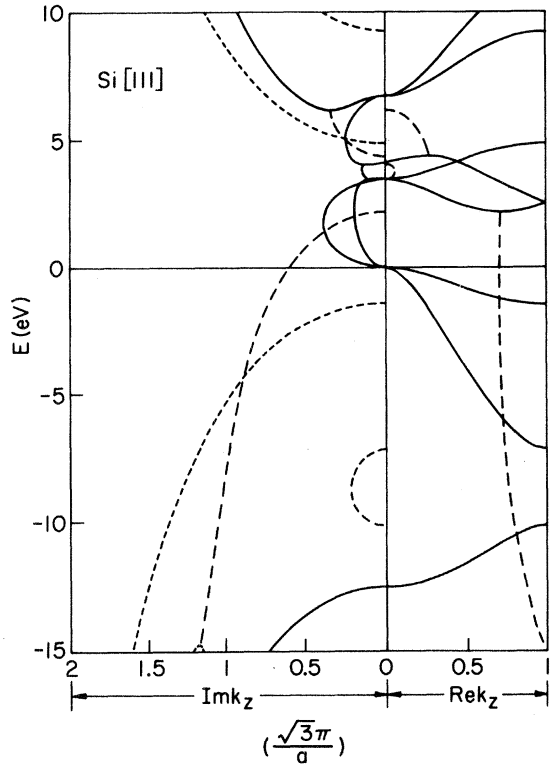

FIG. 3. Complex band structure of Si along [111] direction obtained in the tight-binding scheme. The notation is the same as in Fig. 2.

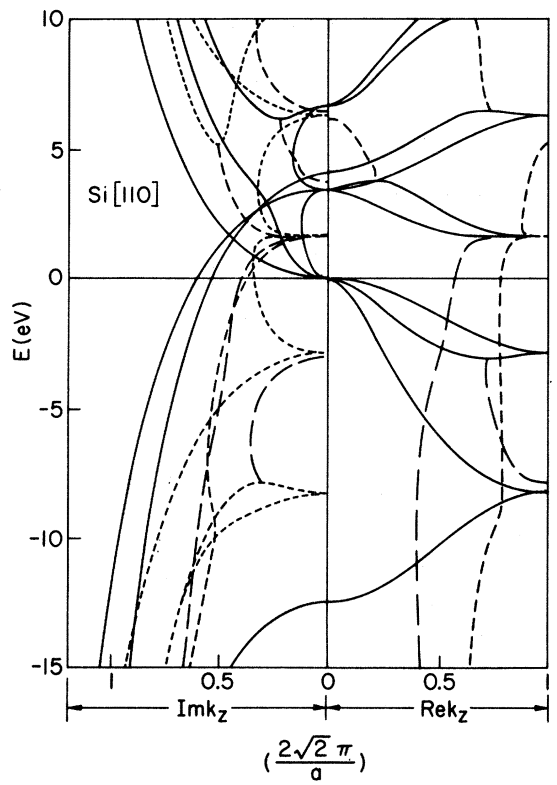

FIG. 4. Complex band structure of Si along [110] direction obtained in the tight-binding scheme. The notation is the same as in Fig. 2.

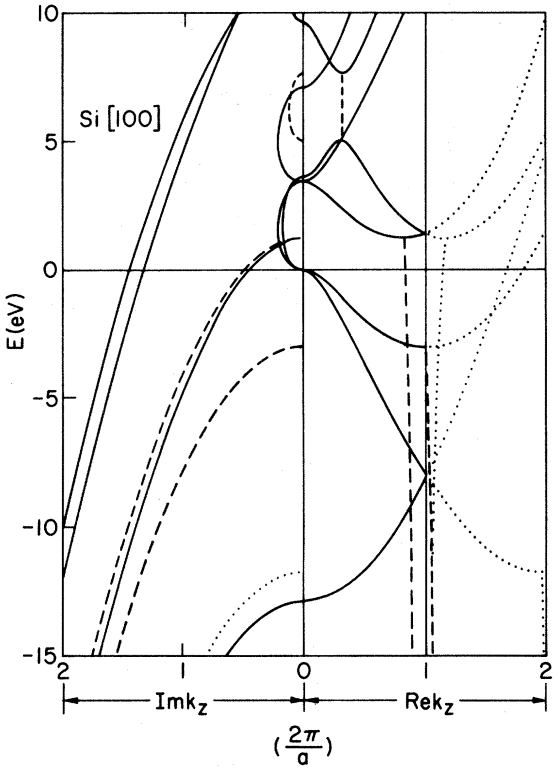

FIG. 5. Complex band structure of Si along [100] direction obtained in the $\vec{k}\cdot\vec{p}$ scheme. Solid curves denote real bands (right) and imaginary bands (left), and dashed curves denote complex bands. Dotted curves denote the repeated solutions, which should be discarded (see text).

values which are separated from the main structures. These bands emanate from conduction-band extrema with energies higher than 10 eV and have little physical significance. Except for these physically insignificant bands, all three schemes seem to produce qualitatively similar complex band structures for energies below 5 eV.

Generally speaking, the complex bands emanating from all the valence bands and the first conduction band produced by the tight-binding scheme are in close agreement with those produced by the pseudopotential scheme, except for some special features in the Si[110] case. In this case two of the three imaginary bands emanating from the valence-band maximum in the pseudopotential scheme join onto the conduction-band minimum. The third goes to $-\infty$, after going through a maximum at $E \sim 0.2$ eV. This maximum and the minimum of the fourth conduction band are connected by a complex band (see Fig. 10). In the tight-binding scheme, only one imaginary band connects up the valence-band maximum and the conduction-band minimum. The other two imaginary bands run monotonically to infinity. The tight-binding scheme does not model the higher conduction bands well; hence, the associated complex bands do not have the same topological structure as those produced in the pseudopotential scheme.

The $\vec{k}\cdot\vec{p}$ scheme appears to be a rather good approximation to the pseudopotential scheme for small values of k_z. Most topological structures of the complex bands near the zone center obtained in the pseudopotential scheme are reproduced quite successfully in this scheme. The major shortcoming of this scheme is the lack of periodicity. This would lead to nonvanishing group velocities for all the bands at the zone boundary. As a result, many imaginary bands of the second kind would become complex bands and any structure involving the connection of a complex band with the extremum of an imaginary band of the second kind would be destroyed. For example, in Fig. 9 (Si[111] within

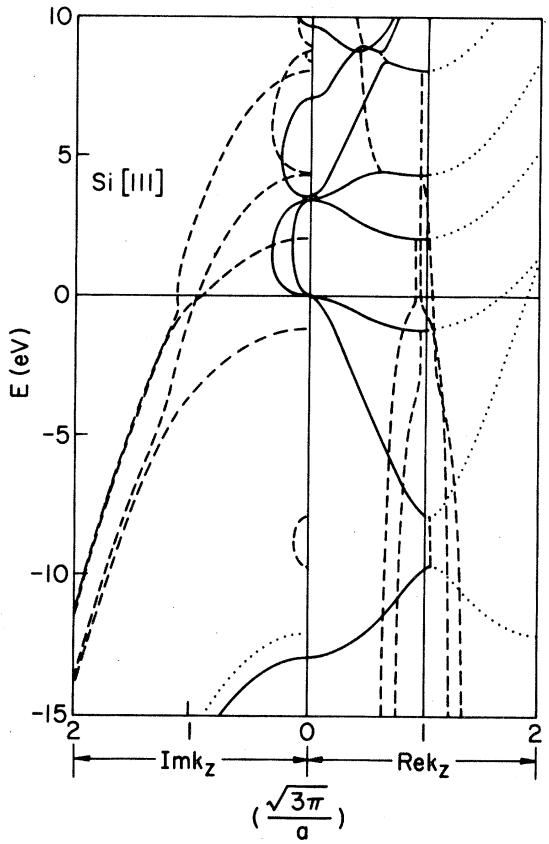

FIG. 6. Complex band structure of Si along [111] direction obtained in the $\vec{k}\cdot\vec{p}$ scheme. The notation is the same as in Fig. 5.

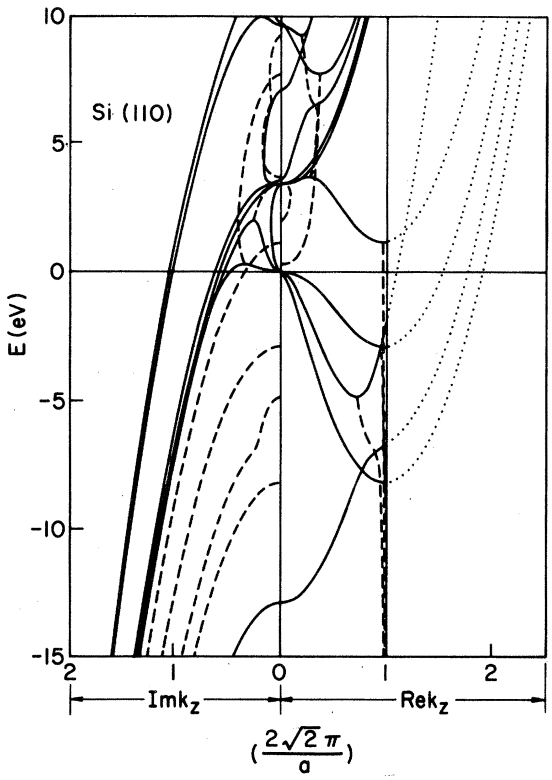

FIG. 7. Complex band structure of Si along [110] direction obtained in the $\vec{k}\cdot\vec{p}$ scheme. The notation is the same as in Fig. 5.

the pseudopotential scheme), the imaginary band of the second kind which connects the first valence band and the second conduction band and the one which connects the first and fifth conduction bands have a minimum near $E\sim-3.0$ and -0.5 eV, respectively. Each of the two minima is connected by a complex band running to $-\infty$. These structures are destroyed in the $\vec{k}\cdot\vec{p}$ scheme as shown in Fig. 6. Similarly, the maximum associated with the imaginary band of the second kind emanating from the lowest valence band (see Figs. 4 and 10) also disappear in the $\vec{k}\cdot\vec{p}$ scheme (Fig. 7). It should be noted that the present $\vec{k}\cdot\vec{p}$ model is designed to produce good overall band structures along the [100] and [111] directions[14]; hence the Si[110] band structure is not well represented, especially for k_z near the zone edge (see Fig. 7). Note that the lowest two valence bands cross each other near $\mathrm{Re}k_z\sim0.8(2\sqrt{2}\pi/2)$ and the second conduction band exceeds 10 eV at the X point, instead of being degenerate with the first conduction band there, as it should be.

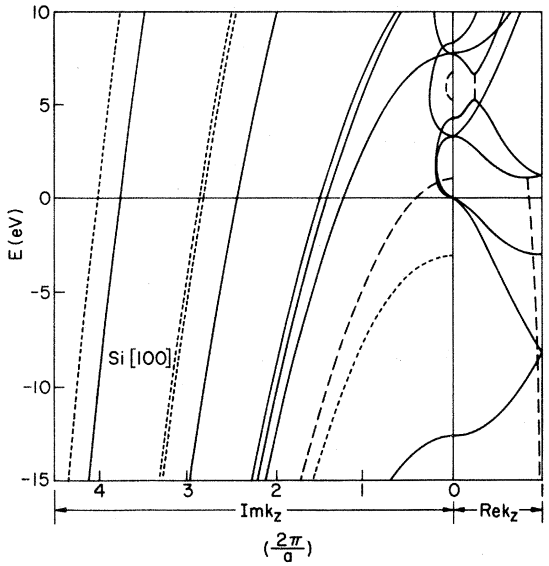

FIG. 8. Complex band structure of Si along [100] direction obtained in the pseudopotential scheme. The notation is the same as in Fig. 2.

IV. GREEN'S FUNCTIONS AND SURFACE STATES

To apply the complex band structure to solid surfaces, we write the surface adapted Green's function, G^0 (i.e., bulk Green's function with fixed $\bar{k}$) in terms of the evanescent states,[9]

$$G^0(\vec{r}\,\vec{r}\,';\bar{k}E)=-2\pi i\left[\sum_\lambda \frac{\psi(\vec{r};\bar{k}k_\lambda^+)\psi(\vec{r}\,';\bar{k}k_\lambda^{+*})}{V_z(\bar{k}k^+)}\Theta(z-z')-\sum_\lambda \frac{\psi(\vec{r};\bar{k}k_\lambda^-)\psi^+(\vec{r}\,';\bar{k}k_\lambda^{-*})}{V_z(\bar{k}k_\lambda^-)}\Theta(z'-z)\right], \quad (28)$$

where the complex k_z solutions are sorted into two groups with $\mathrm{Im}k_\lambda^\pm \gtrless 0$ if $k_\lambda^\pm$ is complex, $V_z(\bar{k}k_\lambda^\pm)\gtrless 0$ if $k_\lambda^\pm$ is real. $\psi(\vec{r};\bar{k}k_\lambda)$ is the Bloch wave function associated with the wave vector $(\bar{k},k_\lambda)$ and

$$V_z(\bar{k}k_\lambda)\equiv\left.\frac{\partial E}{\partial k_z}\right|_{k_z=k_\lambda}$$

is the group velocity of a given complex band. $\Theta(z)$ is a Heaviside step function, with $\Theta(0)\equiv\frac{1}{2}$. We will only present the results obtained in the tight-binding scheme because of its simplicity. In this scheme, the Green's function can be rewritten in the planar orbital basis, i.e.,

$$G^0_{\alpha,\alpha'}(\sigma i,\sigma' i';\bar{k}E)=-2\pi i\left[\sum_\lambda \frac{C_{\alpha i}(k_\lambda^+)C^*_{\alpha' i'}(k_\lambda^{+*})e^{ik_\lambda^+(\sigma-\sigma')a'}}{V_z(\bar{k}k_\lambda^+)}\Theta(\sigma-\sigma')\right.$$

$$\left.-\sum_\lambda \frac{C_{\alpha i}(k_\lambda^-)C^*_{\alpha' i'}(k_\lambda^{-*})e^{ik_\lambda^-(\sigma-\sigma')a'}}{V_z(\bar{k}k_\lambda^-)}\Theta(\sigma'-\sigma)\right], \quad (29)$$

where the $C_{\alpha i}(k_\lambda^\pm)$ are solutions to Eq. (4) with $k_z=k_\lambda^\pm$. $\sigma(\sigma')$ labels the layer, and $i\,(i')$ labels the atomic planes in each layer.

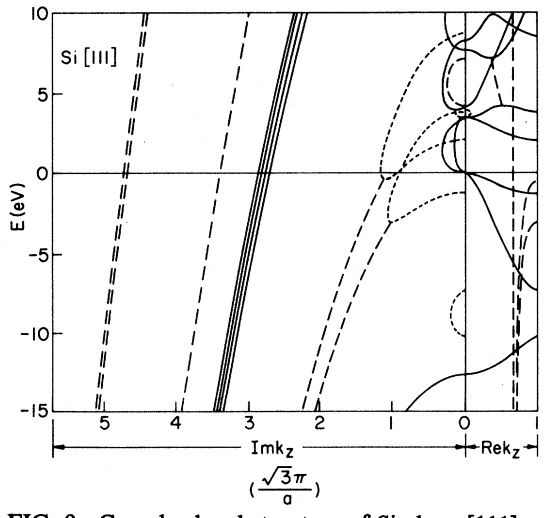

FIG. 9. Complex band structure of Si along [111] direction obtained in the pseudopotential scheme. The notation is the same as in Fig. 2. The three dashed lines in the left panel (with $\mathrm{Im}k_z>3$) are all associated with the dashed line in the right panel with $\mathrm{Re}k_z\simeq 0.67$.

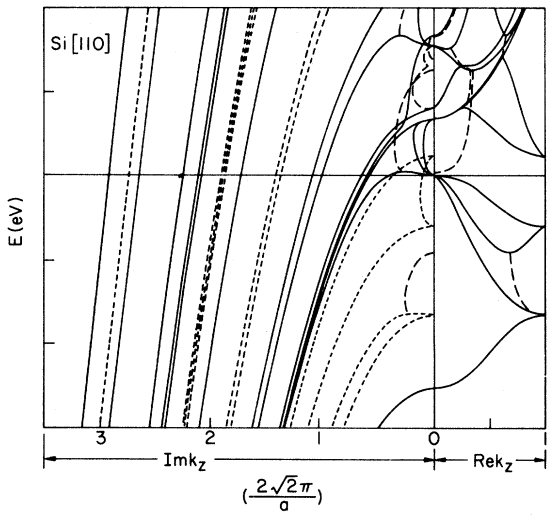

FIG. 10. Complex band structure of Si along [110] direction obtained in the pseudopotential scheme. The notation is the same as in Fig. 2.

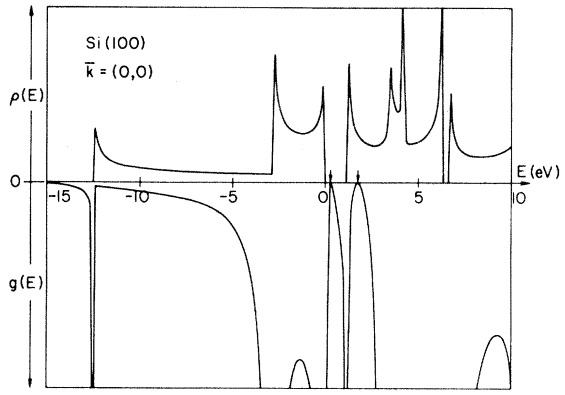

FIG. 11. Surface-wave-vector-resolved local density of states per atomic plane, $\rho(E)$ (upper portion) and real part of the determinant of the bulk Green's function $g(E)$ (lower portion) with $\bar{k}=0$ for the Si(100) face. The arrows indicate the energy positions of the zeros of $g(E)$.

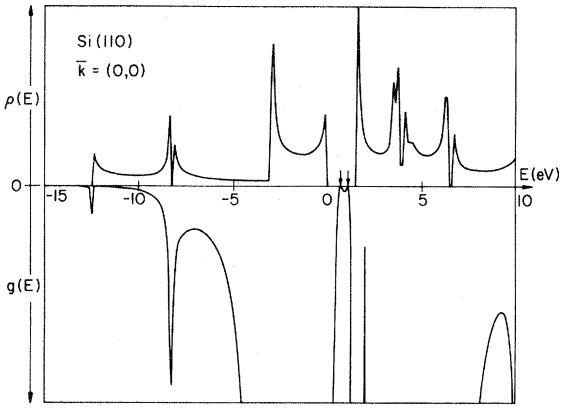

FIG. 13. Same as in Fig. 11 for the Si(110) face.

To evaluate the group velocity $V_z(\vec{k}_\lambda)$, we apply the Hellman-Feynman theorem[17] and obtain

$$V_z(k_\lambda)=\frac{\sum_{\alpha i,\alpha' i'} C^*_{\alpha i}(k^*_\lambda)\left[\frac{\partial}{\partial k_z}H_{\alpha i,\alpha' i'}(k_z)\right]\Big|_{k_z=k_\lambda} C_{\alpha' i'}(k_\lambda)}{\sum_{\alpha i} C^*_{\alpha i}(k^*_\lambda)C_{\alpha i}(k_\lambda)}, \tag{30}$$

where the $H_{\alpha i,\alpha' i'}$ are matrix elements of the Hamiltonian H in the planar orbital basis, written as a function of k_z. In deriving Eq. (30), we have used the property $H(k^*_\lambda)=H^\dagger(k_\lambda)$.[18] With Eqs. (29) and (30), the Green's function is readily evaluated. The results for Si (100), (111), and (110) faces with $\bar{k}=0$ are presented in Figs. 11–13. In Figs. 11–13, the upper portions show the surface-wave-vector-resolved local density of states per atomic plane, $\rho(\bar{k},E)$, which is given by

$$\rho(\bar{k},E)\equiv-\pi\mathrm{Im}[\mathrm{Tr}G^0(\sigma i,\sigma i;\bar{k}E)], \tag{31}$$

and the lower portions show the absolute value of the function

$$g(\bar{k},E)\equiv\mathrm{Re}\{\det[G^0(\sigma i,\sigma i;\bar{k}E)]\}, \tag{32}$$

where G^0 is a five-dimensional matrix for the (100) and (111) faces, and a ten-dimensional matrix for the (110) face. The function $\rho(\bar{k},E)$ has singulari-

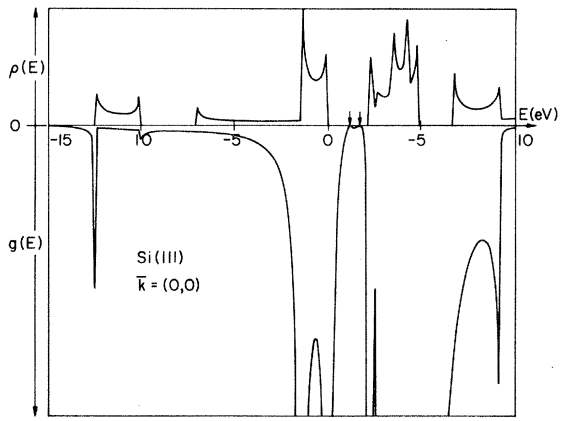

FIG. 12. Same as in Fig. 11 for the Si(111) face.

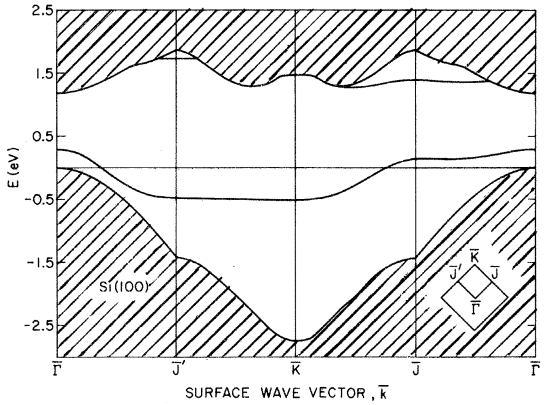

FIG. 14. Surface energy bands of Si(100). The inset shows the surface Brillouin zone.

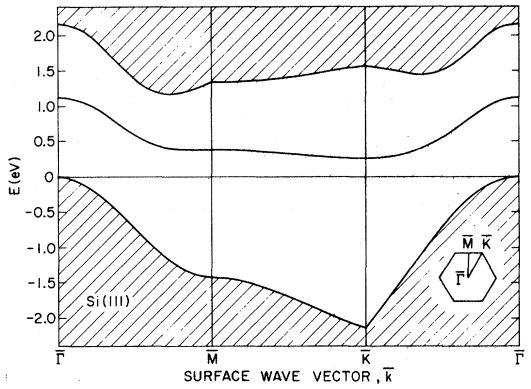

FIG. 15. Surface energy bands of Si(111). The inset shows the surface Brillouin zone.

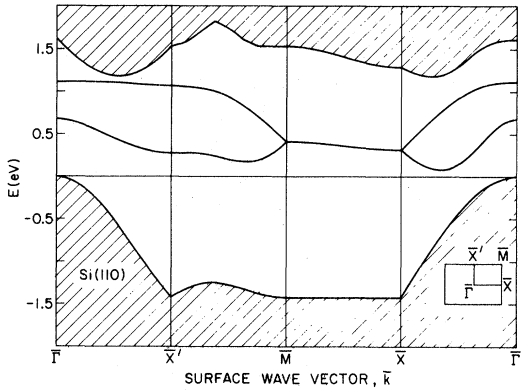

FIG. 16. Surface energy bands of Si(110). The inset shows the surface Brillouin zone.

ties at energies where the group velocity associated with a real band vanishes. The threshold of each peak in Figs. 11—13 can be identified with the corresponding extremum point of the real bands in Figs. 2—4. The function $g(\bar{k},E)$ has singularities at energies where the group velocity associated with any complex band (including the real one) vanishes. Furthermore, according to the orbital removal method[8] the zeros of $g(\bar{k},E)$ correspond to the energy positions of the surface states (if E is in the gap) or surface resonances (if E is not in the gap) for the ideal surface. The positions of these zeros are marked by arrows in Figs. 11—13.

Tracing the thresholds of $\rho(\bar{k},E)$ and the zeros of $g(\bar{k},E)$ for different values of $\bar{k}$, we obtain the projected band structures and dispersion curves of the surface states for the ideal Si (100), (111), and (110) surfaces. The results within the fundamental gap are shown in Figs. 14—16. It should be noted that the removal of one plane of atomic orbitals results in two surfaces. For the Si(100) and Si(110) cases, these two surfaces are identical; therefore, all zeros of $g(\bar{k},E)$ are doubly degenerate. For the Si(111) case, one surface has one dangling bond and other has three dangling bonds (which is a nonphysical surface). To identify the zeros of $g(\bar{k},E)$ with the two nonidentical Si(111) surfaces, we check the determinant of the Green's function corresponding to the removal of two atomic planes (which results in two identical surfaces, having either one or three dangling bonds). In Fig. 12, the zero at $g(E)$ with lower energy indicates the surface state of the one-dangling-bond surface, the other indicates that of the three-dangling-bond surface. In Fig. 15, only the surface states of the surface with one dangling bond are shown. The results for the ideal Si(111) surface are identical to those obtained by Buisson *et al.*[19] In Ref. 19 the spectral representation (conventional technique) for the bulk Green's function was used and the creation of the surface is modeled by cutting a plane of chemical bonds. We find that the current technique is at least an order of magnitude more efficient than the conventional technique[8,19] and easier to implement. Furthermore, the present technique calculates the bulk Green's function exactly for each fixed $\bar{k}$ and E, whereas the conventional one only does it approximately.

V. SUMMARY

We have presented a method for finding the complex k_z solutions (evanescent states) to the bulk Schrödinger equation for arbitrary faces of a crystalline solid. This method is simple, efficient, and free of numerical difficulties. Furthermore, it is adaptable to the pseudopotential, the $\vec{k}\cdot\vec{p}$, as well as the tight-binding schemes. To illustrate the use of this method, we have calculated the complex band structures of Si in all the three schemes and examined their differences.

The complex band structures have many useful applications to the crystalline solid involving a planar defect. Several of these applications, in which the wave-function matching method was used, were discussed previously for solid surfaces,[1—3] interfaces[4] and superlattices.[5] In the present paper, we have demonstrated that by incorporating the complex band structures with the analytical representation of the bulk Green's function,[9] one can calculate the surface electronic properties with great efficiency. The simplicity and efficiency of this technique should offer prom-

ise of solving more complicated problems related to planar defects in solids, such as surfaces with a large unit-mesh reconstruction [e.g., the Si(111)-(7×7) reconstruction], surfaces or interfaces with relaxations extended to many layers, and large size defects (e.g., dislocations or steps) on surfaces. Research along these lines is currently in progress.

ACKNOWLEDGMENTS

We would like to acknowledge many fruitful discussions with R. E. Allen and J. P. Buisson. This work was supported in part by the Materials Research Laboratory under Contract Nos. NSF-DMR-80-20250 and DOE-DE-AC02-76ER01198.

---

*Present address: Department of Physics and Astronomy, University of Hawaii, Honolulu, Hawaii 96822.

[1]V. Heine, Proc. Phys. Soc. London 81, 30 (1963).

[2]R. O. Jones, Proc. Phys. Soc. London 89, 443 (1966); Phys. Rev. Lett. 20, 992 (1968).

[3]F. Forstmann and V. Heine, Phys. Rev. Lett. 24, 1419 (1970).

[4]G. C. Osbourn and D. L. Smith, Phys. Rev. B 19, 2124 (1979).

[5]J. N. Schulman and Y. C. Chang, Phys. Rev. B 24, 4445 (1981).

[6]K. C. Pandey and J. C. Phillips, Phys. Rev. Lett. 32, 1433 (1974); 34, 1450 (1975); Phys. Rev. B 13, 750 (1976).

[7]G. F. Koster and J. C. Slater, Phys. Rev. 95, 1167 (1954).

[8]J. Pollmann, in *Advances in Solid State Physics,* edited by J. T. Treusch (Vieweg, Braunschweig, 1980), p. 117 and references therein.

[9]R. E. Allen, Phys. Rev. B 19, 917 (1979); 20, 1454 (1979).

[10]Y. C. Chang, Phys. Rev. B 25, 605 (1982).

[11]A similar method for solving the polynomial equation for the lattice vibrational problem has been presented in H. Matsuda, K. Okada, T. Takase, and T. Yamamoto, J. Chem. Phys. 41, 1527 (1964).

[12]D. H. Lee and J. D. Joannopoulos, Phys. Rev. B 23, 4988 (1981); 23, 4997 (1981).

[13]J. R. Chelikowsky and M. L. Cohen, Phys. Rev. B 14, 556 (1976).

[14]M. Cardona and F. H. Pollak, Phys. Rev. 142, 530 (1966).

[15]This was previously pointed out by I. Alstrup, Surf. Sci. 20, 335 (1970).

[16]P. Vogl, H. P. Hjalmarson, and J. D. Dow, J. Phys. Chem. Sol. (in press); see also H. P. Hjalmarson, Ph.D. thesis, University of Illinois at Urbana-Champaign, 1979 (unpublished).

[17]See for example, E. Merzbacher, *Quantum Mechanics,* 2nd ed. (Wiley, New York, 1970), p. 442.

[18]E. I. Blount, in *Solid State Physics,* edited by F. Seitz and D. Turnbull (Academic, New York, 1962), Vol. 13, p. 305.

[19]J. P. Buisson, R. E. Allen, and J. D. Dow (unpublished).